

Possible effects of the large extra dimensions on ZZW production at the LHC

Chen Chong, Guo Lei, Ma Wen-Gan, Zhang Ren-You, Li Xiao-Zhou, and Zhang Yu
Department of Modern Physics, University of Science and Technology of China (USTC),
Hefei, Anhui 230026, People's Republic of China

Abstract

We investigate the possible large extra dimensions (LED) effects induced by the Kaluza-Klein gravitons up to the QCD next-to-leading order (NLO) on ZZW production at the large hadron collider (LHC). The integrated cross sections and some kinematic distributions are presented in both the standard model (SM) and the LED model. The numerical results demonstrate that the NLO QCD corrections are sizeable and remarkably reduce the leading order (LO) LED effect depending strongly on the phase space. The NLO LED relative discrepancies of the total cross section could become sizable for the ZZW production, if we apply proper event selection criteria. We find that the LO result overestimates the LED effect and is insufficient to provide a believable theoretical prediction.

PACS: 11.10.Kk, 14.70.Fm, 14.70.Hp

I. Introduction

To solve the long-standing hierarchy problem, many exciting extensions of the standard model (SM) have been developed, such as supersymmetric models, little Higgs models, extra dimension models, and etc. Among these extensions, the large extra dimensions (LED) model proposed by Arkani-Hamed, Dimopoulos and Dvali [1, 2, 3] is an attractive one because it predicts possible quantum gravity effects at TeV scale. In the LED model, we have $(4 + d)$ -dimensional spacetime with d being the number of extra spatial dimensions compactified on a d -dimensional torus with radius R . The SM particles are confined on a 4-dimensional brane world while the graviton can propagate in the $(4 + d)$ -dimensional bulk. The Planck scale M_P in the 4-dimensional spacetime is related to the fundamental scale M_S of the LED model as $M_P^2 = R^d M_S^{d+2}$. If R is large enough, the gravity interaction governed by M_S and the gauge interaction can be unified at the TeV scale, therefore, the gauge hierarchy problem is solved.

In the low-energy effective theory of the LED model, the massless graviton propagating in the $(4 + d)$ -dimensional spacetime is equal to a tower of massive Kaluza-Klein (KK) states only propagating in the ordinary 4-dimensional spacetime [4]. After performing the KK reduction, we obtain the 4-dimensional interactions of the SM particles with the KK gravitons. These effective couplings are heavily suppressed by $1/\overline{M}_P$, where \overline{M}_P is the reduced Planck scale defined as $\overline{M}_P = M_P/\sqrt{8\pi}$. However, for both the virtual graviton exchange and the real graviton production, the summation over the tower of KK states cancels the dependence on \overline{M}_P and leads to a suppression of the order of M_S . Therefore, the KK-graviton effects may be considerable at high energy colliders.

The triple gauge boson (TGB) productions are of particular interest because they are sensitive to the quartic gauge couplings (QGCs) and thus related to the electroweak symmetry breaking (EWSB) mechanism [5, 6]. Any deviation from the SM predictions would hint at the existence of new physics. Therefore, the precision studies on the TGB productions at high energy colliders within all the possible new physics models are necessary in discriminating physics beyond the SM. All the TGB productions at hadron colliders have been studied in the SM up to the QCD next-to-leading order (NLO). It is found that the NLO QCD corrections are sizable, strongly depend on the phase space and significantly exceed the expectations from a scale variation of the leading order (LO) result. Therefore, the NLO QCD corrections should be taken into account for the TGB production phenomenological study.

The CERN Large Hadron Collider (LHC) is expected to explore the mechanism of EWSB and new physics evidences at the TeV scale, and provide more precision measurements of the QGCs than the existing data from LEP II and Tevatron [7, 8]. Compared with the thoroughly studied TGB productions at hadron colliders in the SM, only the $pp \rightarrow \gamma\gamma\gamma, \gamma\gamma Z, \gamma ZZ, ZZZ, W^+W^-\gamma, W^+W^-Z$ processes at the LHC were studied at the LO in the framework of the LED model [9, 10]. As the ZZW production is directly related to the ZZW^+W^- QGC, the precision theoretical predictions on the ZZW production are needed for the measurement of the ZZW^+W^- coupling and the search for the new physics signature in experiment. Recently, the generalized effective W approximation is applied to study the WW scattering based on the factorization [11]. In this paper, we investigate the possible LED effects on the ZZW production at the CERN LHC up to the QCD NLO. The rest of the paper is organized as follows. In Sec. II, the calculation strategy is presented. In Sec. III, the numerical results and discussions are provided. Finally, a short summary is given in Sec. IV.

II. Calculation strategy

II.1 Related LED theory

In this work we adopt the de Donder gauge and Feynman gauge for the KK-graviton part and SM part, respectively. The related Feynman rules used in our calculations are listed in Table 1, where $G_{\text{KK}}^{\mu\nu}$, ψ , $A^{a\mu}$, $W^{\pm\mu}$ and Z^μ represent the fields of the graviton, quark, gluon, W -boson and Z -boson, respectively. The momenta of KK graviton and gauge bosons are set to be into vertex, while the quark momentum is defined in the direction of the quark flow [4]. α_3 and ξ are the $SU(3)$ and charged $SU(2)$ gauge fixing parameters which are taken as $\alpha_3 = \xi = 1$ in Feynman gauge. $\kappa = \sqrt{2}/M_P$ is the gravity coupling constant. $D(s)$ in the KK-graviton propagator can be expressed as [4]

$$D(s) = \frac{16\pi}{\kappa^2} \frac{s^{d/2-1}}{M_S^{d+2}} \left[\pi + 2iI(\Lambda/\sqrt{s}) \right], \quad (2.1)$$

where

$$I(\Lambda/\sqrt{s}) = P \int_0^{\Lambda/\sqrt{s}} dy \frac{y^{d-1}}{1-y^2}. \quad (2.2)$$

The integral $I(\Lambda/\sqrt{s})$ contains an ultraviolet cutoff Λ on the KK modes [4, 12] and in our calculations we set Λ to be the fundamental scale M_S routinely. The tensor coefficients $B^{\mu\nu\alpha\beta}$, $C^{\rho\sigma\mu\alpha\beta}$ and $E^{\mu\nu\rho\sigma}(k_1, k_2)$

are given by [13]

$$\begin{aligned}
B^{\mu\nu\alpha\beta} &= \frac{1}{2}(\eta^{\mu\nu}\eta^{\alpha\beta} - \eta^{\mu\alpha}\eta^{\nu\beta} - \eta^{\mu\beta}\eta^{\nu\alpha}), \\
C^{\rho\sigma\mu\nu\alpha\beta} &= \frac{1}{2}[\eta^{\rho\sigma}\eta^{\mu\nu}\eta^{\alpha\beta} - (\eta^{\rho\mu}\eta^{\sigma\nu}\eta^{\alpha\beta} + \eta^{\rho\nu}\eta^{\sigma\mu}\eta^{\alpha\beta} + \eta^{\rho\alpha}\eta^{\sigma\beta}\eta^{\mu\nu} + \eta^{\rho\beta}\eta^{\sigma\alpha}\eta^{\mu\nu})], \\
E^{\mu\nu\rho\sigma}(k_1, k_2) &= \eta^{\mu\nu}(k_1^\rho k_1^\sigma + k_2^\rho k_2^\sigma + k_1^\rho k_2^\sigma) - [\eta^{\nu\sigma}k_1^\mu k_1^\rho + \eta^{\nu\rho}k_2^\mu k_2^\sigma + (\mu \leftrightarrow \nu)].
\end{aligned} \tag{2.3}$$

We code the related Feynman rules of the LED model in the FeynArts-3.5 package [14] to generate the Feynman diagrams and the corresponding amplitudes. Our developed FormCalc-5.4 package [15] is used subsequently to simplify the amplitudes. In the following, we present the calculation details of different contribution parts to the ZZW production at the LO and QCD NLO, and the verification of the consistency of our results with previous publications [16, 17].

Vertex	Feynman rule
$G_{\text{KK}}^{\mu\nu}(k_3)A^{a\rho}(k_1)A^{b\sigma}(k_2)$	$-i\kappa\left[(C^{\mu\nu\rho\sigma\tau\beta} - C^{\mu\nu\rho\beta\sigma\tau})k_{1\tau}k_{2\beta} + \frac{1}{\alpha_3}E^{\mu\nu\rho\sigma}(k_1, k_2)\right]\delta^{ab}$
$G_{\text{KK}}^{\mu\nu}(k_3)W^{+\rho}(k_1)W^{-\sigma}(k_2)$	$-i\kappa\left[(C^{\mu\nu\rho\sigma\tau\beta} - C^{\mu\nu\rho\beta\sigma\tau})k_{1\tau}k_{2\beta} + \frac{1}{\xi}E^{\mu\nu\rho\sigma}(k_1, k_2) + B^{\mu\nu\rho\sigma}m_W^2\right]$
$G_{\text{KK}}^{\mu\nu}(k_3)Z^\rho(k_1)Z^\sigma(k_2)$	$-i\kappa\left[(C^{\mu\nu\rho\sigma\tau\beta} - C^{\mu\nu\rho\beta\sigma\tau})k_{1\tau}k_{2\beta} + \frac{1}{\xi}E^{\mu\nu\rho\sigma}(k_1, k_2) + B^{\mu\nu\rho\sigma}m_Z^2\right]$
$G_{\text{KK}}^{\mu\nu}(k_3)\bar{\psi}(k_1)\psi(k_2)$	$-i\frac{\kappa}{8}\left[\gamma^\mu(k_1 + k_2)^\nu + \gamma^\nu(k_1 + k_2)^\mu - 2\eta^{\mu\nu}(\not{k}_1 + \not{k}_2 - 2m_\psi)\right]$
$G_{\text{KK}}^{\mu\nu}(k_4)\bar{\psi}_{u_i}(k_1)\psi_{d_j}(k_2)W^{+\rho}(k_3)$	$-ie\frac{\kappa}{4\sqrt{2}\sin\theta_W}(\gamma^\mu\eta^{\nu\rho} + \gamma^\nu\eta^{\mu\rho} - 2\gamma^\rho\eta^{\mu\nu})V_{CKM}^{ij}$
$G_{\text{KK}}^{\mu\nu}(k_4)\bar{\psi}(k_1)\psi(k_2)A^{a\rho}(k_3)$	$ig_s\frac{\kappa}{4}(\gamma^\mu\eta^{\nu\rho} + \gamma^\nu\eta^{\mu\rho} - 2\gamma^\rho\eta^{\mu\nu})T^a$
Spin-2 KK-graviton propagator after summation over KK states:	
$\tilde{G}_{\text{KK}}^{\mu\nu\alpha\beta} = \frac{1}{2}D(s)\left[\eta^{\mu\alpha}\eta^{\nu\beta} + \eta^{\mu\beta}\eta^{\nu\alpha} - \frac{2}{d+2}\eta^{\mu\nu}\eta^{\alpha\beta}\right]$	

Table 1: Related LED Feynman rules used in this work.

II.2 LO cross section

We neglect the masses of u -, d -, c -, s -quarks and the quark mixing between the third generation and the first two generations. Due to the smallness of the b -quark parton density in the proton, only the $qq' \rightarrow ZZW^+$ ($qq' = u\bar{d}, u\bar{s}, c\bar{d}, c\bar{s}$) and $qq' \rightarrow ZZW^-$ ($qq' = \bar{u}d, \bar{u}s, \bar{c}d, \bar{c}s$) partonic processes are involved in the ZZW^+ and ZZW^- productions at the LHC, respectively. At parton level, the cross section for the ZZW^- production is the same as that for the ZZW^+ production due to the CP conservation. In

in this section we present only the analytical results for the $pp \rightarrow ZZW^+ + X$ process. The LO Feynman amplitude for the partonic process $qq' \rightarrow ZZW^+$ can be expressed as

$$\mathcal{M}_{qq'}^{LO} = \mathcal{M}_{qq'}^{SM} + \mathcal{M}_{qq'}^{LED}, \quad (2.4)$$

where $\mathcal{M}_{qq'}^{SM}$ and $\mathcal{M}_{qq'}^{LED}$ are the amplitudes contributed by the SM-like diagrams and the KK-graviton exchange diagrams, respectively. The LO Feynman diagrams involving KK-graviton exchange are shown in Fig.1. The LO cross section for $qq' \rightarrow ZZW^+$ has the form as

$$\hat{\sigma}_{qq'}^0 = \frac{1}{4|\vec{p}|\sqrt{\hat{s}}} \int \sum' |\mathcal{M}_{qq'}^{LO}|^2 d\Omega_3, \quad (2.5)$$

where \vec{p} is the three-momentum of one initial parton in the center-of-mass system (c.m.s.), $\sqrt{\hat{s}}$ is the c.m.s. colliding energy, $d\Omega_3$ is the three-body phase space element, the summation is taken over the spins and colors of the initial and final states, and the prime on the summation indicates averaging over the intrinsic degrees of freedom of initial partons. By convoluting $\hat{\sigma}_{qq'}^0$ with the parton distribution functions (PDFs) of the colliding protons, we obtain the LO total cross section for the parent process $pp \rightarrow ZZW^+ + X$ as

$$\sigma_{LO} = \sum_{qq'=u\bar{d},u\bar{s}}^{c\bar{d},c\bar{s}} \int_0^1 dx_1 dx_2 \left[G_{q/P_1}(x_1, \mu_f) G_{q'/P_2}(x_2, \mu_f) \hat{\sigma}_{qq'}^0(\sqrt{\hat{s}} = x_1 x_2 \sqrt{s}) + (1 \leftrightarrow 2) \right], \quad (2.6)$$

where $G_{q/P}$ represents the PDF of parton q in proton P , x_i ($i = 1, 2$) describes the momentum fraction of a parton in proton, \sqrt{s} is the colliding energy in the rest frame of proton-proton system, and μ_f is the factorization scale.

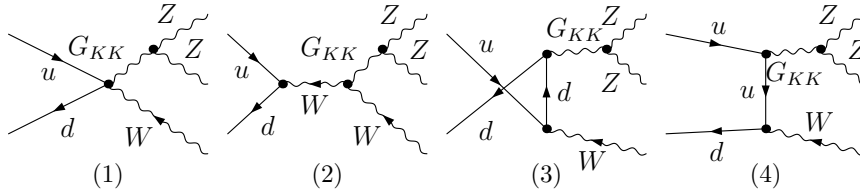


Figure 1: The LO Feynman diagrams with KK-graviton exchange for the partonic process $u\bar{d} \rightarrow ZZW^+$.

II.3 Virtual corrections

There are 145 QCD one-loop Feynman diagrams for the $qq' \rightarrow ZZW^+$ partonic process, including 22 boxes and 6 pentagons. These loop diagrams contain both UV and IR singularities. All the UV and part

of the IR divergences can be removed after performing the renormalization procedure by introducing the quark wavefunction renormalization constants $\delta Z_{q,L}$ and $\delta Z_{q,R}$ which are fixed in the modified minimal subtraction (\overline{MS}) renormalization scheme as

$$\delta Z_{q,L} = \delta Z_{q,R} = -\frac{\alpha_s(\mu_r)}{4\pi} C_F (\Delta_{UV} - \Delta_{IR}), \quad (2.7)$$

where $C_F = \frac{4}{3}$, μ_r is the renormalization scale, and $\Delta_{UV} = \frac{1}{\epsilon_{UV}} \Gamma(1 + \epsilon_{UV}) (4\pi)^{\epsilon_{UV}}$ and $\Delta_{IR} = \frac{1}{\epsilon_{IR}} \Gamma(1 + \epsilon_{IR}) (4\pi)^{\epsilon_{IR}}$ refer to the UV and IR divergences regulated in the dimensional regularization scheme, respectively. The residual IR divergences can be canceled by adding the contributions of the real emission processes and the corresponding PDF counterterms.

In deduction of the Feynman amplitudes, the 3- and 4-point tensor integrals are recursively reduced to scalar integrals using Passarino-Veltman (PV) method [18], while the 5-point integrals are reduced to 4-point integrals by using the method proposed by Denner and Dittmaier [19]. We should address that the rank $n > 3$ tensor 4-point integrals may induce a serious unstable problem in the numerical calculation. One way to solve this problem is to adopt quadruple precision arithmetic in the numerical calculation of loop integrals, but the cost is obvious to consume much more computer CPU time. In order to improve the efficiency of the calculation, we adopt the segmentation method analogous to that in Ref.[20, 21] to treat the unstable problem. We developed the codes for the calculation of the scalar and tensor integrals based on the LoopTools-2.7 package, which can switch to the quadruple precision codes automatically in the region of

$$\frac{\det G_3}{(2k_{max}^2)^3} < 10^{-5}, \quad (2.8)$$

where $\det G_3$ is the Gram determinant and k_{max}^2 the maximum of the external four-momentum squared for a given 4-point integral. The calculation speed by using our modified LoopTools is about ten times faster than that using pure quadruple precision arithmetic in the whole phase space.

II.4 Real emission corrections

We employ the dipole subtraction (DS) scheme proposed by Catani and Seymour to deal with the IR singularities in the real emission corrections. [22]. In the DS scheme, the real emission correction $d\sigma_R$ is subtracted by the dipole term $d\sigma_{DP}$ before integration over the $(m+1)$ -body phase space¹. The dipole

¹ $m = 3$ for ZZW production.

term approximates the divergent behavior of the real emission in all soft/collinear regions, which means $(d\sigma_R - d\sigma_{DP})$ is finite and can be integrated in four dimensions directly. Then the NLO QCD corrected cross section can be expressed as

$$\sigma_{NLO} = \sigma_{LO} + \int_m \left[d\sigma_V + d\sigma_{PDF} + \int_1 d\sigma_{DP} \right] + \int_{m+1} \left[d\sigma_R - d\sigma_{DP} \right], \quad (2.9)$$

where $d\sigma_V$ and $d\sigma_{PDF}$ are the virtual correction and the contribution of the PDF counterterms, respectively. The integration over the real emission particle phase space $\int_1 d\sigma^{DP}$ can be computed analytically. As mentioned above, the IR divergences in $d\sigma_V$ can be canceled by those in $d\sigma_{PDF}$ and $\int_1 d\sigma^{DP}$. The integration of $(d\sigma_V + d\sigma_{PDF} + \int_1 d\sigma_{DP})$ over the m -body phase space can also be performed numerically in four dimensions.

The real emission corrections to the $pp \rightarrow ZZW^+ + X$ process are from the real gluon emission processes $qq' \rightarrow ZZW^+g$ ($qq' = u\bar{d}, u\bar{s}, c\bar{d}, c\bar{s}$) and the real light-quark emission processes $gq \rightarrow ZZW^+q'$ ($qq' = ud, \bar{d}\bar{u}, us, \bar{s}\bar{u}, cd, \bar{d}\bar{c}, cs, \bar{s}\bar{c}$). In the case of real gluon emission two dipoles are needed as subtraction terms, while for the case of real light-quark emission, only one subtraction term is needed. The analytical expressions for the dipoles are presented in Ref.[17].

In the numerical calculation using the subtraction scheme, we will encounter the so-called missed binning problem [23], because a huge positive weight from the real emission part and the corresponding huge negative weight from the subtraction term may be filled into different histogram bins. In Ref.[23], Zoltan Nagy introduces a parameter α , which decreases the size of dipole phase space, to distinct regions neighboring a singularity and regions without need of a subtraction. We may suppress missed binning by taking proper value of α .

In Table 2 we make the comparison between our numerical results for the ZZW^+ production and those from Refs.[16] and [17] in the SM for some typical values of the factorization/renormalization scale. We take all the input parameter values being the same as in Refs.[16, 17]. From Table 2 we can see that our LO and NLO results are in agreement with those provided in Ref.[16], and both the results of Ref.[16] and ours are coincident at the 1% level with those given in Ref.[17].

III. Numerical results and discussions

III..1 Input parameters

In our numerical calculations, the SM input parameters are taken as $\alpha_{\text{ew}}^{-1} = 137.035999074$, $m_W = 80.385$ GeV, $m_Z = 91.1876$ GeV [24] and $m_H = 126$ GeV [25, 26]. Since the LED model is a low-energy effective theory, it breaks down when $\sqrt{p_G^2} \gtrsim M_S$, where p_G is the four-momentum flowing through the KK graviton. For ZZW production, p_G^2 is the invariant mass squared of final Z -boson pair. The factorization and renormalization scales are set to be equal and the central value of the factorization/renormalization scale is defined as $\mu_0 = 2m_Z + m_W$. In order to make reliable and viable phenomenological predictions, we take the hard and conservative truncation scheme by applying the cut $M_{ZZ} < M_S$. For the initial state convolution, we adopt CTEQ6L1 PDFs with $\Lambda_5^{LO} = 165$ MeV and CTEQ6M PDFs [27] with $\Lambda_5^{\overline{MS}} = 226$ MeV in the LO and NLO calculations, respectively. The Cabibbo-Kobayashi-Maskawa (CKM) matrix elements are taken as

$$V_{CKM} = \begin{pmatrix} V_{ud} & V_{us} & V_{ub} \\ V_{cd} & V_{cs} & V_{cb} \\ V_{td} & V_{ts} & V_{tb} \end{pmatrix} = \begin{pmatrix} 0.97425 & 0.22547 & 0 \\ -0.22547 & 0.97425 & 0 \\ 0 & 0 & 1 \end{pmatrix}. \quad (3.1)$$

Up to now, the ATLAS and CMS Collaborations at the LHC have not yet observed the signature of extra spatial dimensions. All the experimental data are in good agreement with the SM predictions and thus provide more severe constraints on the LED parameters. The ATLAS Collaboration provided lower limits on M_S at 95% confidence level (CL) between 2.4 TeV and 3.9 TeV in dilepton events at

μ [GeV]	data source	σ_{LO} [fb]	σ_{NLO} [fb]
$\frac{3}{2} m_Z$	Ours	20.46(1)	42.91(2)
	Ref.[16]	20.42(3)	43.02(8)
	Ref.[17]	20.2(1)	43.0(2)
$2 m_Z + m_W$	Ours	20.31(1)	39.98(2)
	Ref.[16]	20.30(3)	39.87(9)
	Ref.[17]	20.2(1)	40.4(2)
$3 m_Z$	Ours	20.30(1)	39.83(2)
	Ref.[16]	20.24(3)	39.86(7)
	Ref.[17]	20.0(1)	39.7(2)
$6 m_Z$	Ours	20.07(1)	37.40(1)
	Ref.[16]	20.03(3)	37.39(7)
	Ref.[17]	19.7(1)	37.8(2)

Table 2: The comparison between our SM results and those from Refs.[16] and [17] for ZZW^+ production at the $\sqrt{s} = 14$ TeV LHC.

$\sqrt{s} = 7$ TeV LHC depending on the choice of model, channel and prior. After combining the dilepton and diphoton searches, the limits are in the range of 2.6 – 4.2 TeV [28, 29]. While the CMS Collaboration set the M_S lower limits of up to 4.77 TeV at 95% CL in dielectron events, depending on the number of extra dimensions and the validity range of the theory [30]. In discussing the LED effects, we apply two event selection schemes. In scheme (I) we collect all the events without any cut on the final products, while in scheme (II) we only accept the events satisfying the following event selection criteria:

$$M_{ZZ} > 500 \text{ GeV}, \quad p_T^Z > 100 \text{ GeV}, \quad p_T^W > 20 \text{ GeV}. \quad (3.2)$$

In our calculations the LED parameters are taken as $M_S = 4.8$ TeV, $d = 3$ and adopt scheme (II) for event selection unless otherwise stated.

III..2 Production cross section

In Table 3 we present the integrated cross sections and the corresponding QCD K -factor in the SM and the LED model, and the LED relative discrepancy δ which is defined as $\delta = (\sigma_{LED} - \sigma_{SM})/\sigma_{SM}$, for the ZZW^+ and ZZW^- productions in the event selection scheme (I) at the $\sqrt{s} = 14$ TeV LHC. The LO relative deviations between the total cross sections predicted in the LED model and the SM for the ZZW^+ and ZZW^- productions are 2.40% and 1.23%, respectively. Like most of the TGB production processes, the LO cross sections for the ZZW^+ and ZZW^- productions are enhanced significantly by the NLO QCD corrections, but the QCD corrections strongly reduce the LO LED relative discrepancies and make the NLO relative deviations down to 1.03% and 0.65%, respectively. In other words, the LO result overestimates the LED effect and the NLO LED signal in scheme (I) is almost submerged in the SM background with our chosen parameters.

	ZZW^+			ZZW^-		
	$\sigma_{LO} (fb)$	$\sigma_{NLO} (fb)$	K	$\sigma_{LO} (fb)$	$\sigma_{NLO} (fb)$	K
SM	18.29(1)	36.84(2)	2.014	9.428(4)	20.01(1)	2.122
LED	18.73(1)	37.22(2)	1.987	9.544(4)	20.14(1)	2.110
δ	2.40%	1.03%	—	1.23%	0.65%	—

Table 3: Integrated cross sections in scheme (I) for the $pp \rightarrow ZZW^\pm + X$ processes in the SM and the LED model at the $\sqrt{s} = 14$ TeV LHC with $\mu = \mu_0 = 2m_Z + m_W$, $M_S = 4.8$ TeV and $d = 3$.

In Table 4 we provide the results by taking the event selection scheme (II) with the same input

parameters as in Table 3. The results in scheme (II) show that both the LO and NLO LED relative discrepancies between the SM and LED predictions increase significantly. The LO (NLO) LED relative deviations reach the values of 19.88% (8.05%) and 12.30% (5.63%) for the ZZW^+ and ZZW^- productions, respectively. Here we see also that the LO prediction overestimates the LED relative deviation for the ZZW production at the LHC.

	ZZW^+			ZZW^-		
	$\sigma_{LO} (fb)$	$\sigma_{NLO} (fb)$	K	$\sigma_{LO} (fb)$	$\sigma_{NLO} (fb)$	K
SM	2.062(1)	4.372(6)	2.120	0.878(1)	2.025(4)	2.306
LED	2.472(2)	4.724(7)	1.911	0.986(1)	2.139(4)	2.169
δ	19.88%	8.05%	—	12.30%	5.63%	—

Table 4: Integrated cross sections in scheme (II) for the $pp \rightarrow ZZW^\pm + X$ processes in the SM and the LED model at the $\sqrt{s} = 14$ TeV LHC with $\mu = \mu_0 = 2m_Z + m_W$, $M_S = 4.8$ TeV and $d = 3$.

III..3 Scale dependence

We depict the LO, NLO QCD corrected total cross sections and the corresponding K -factors for the ZZW^+ and ZZW^- productions in the LED model at the $\sqrt{s} = 14$ TeV LHC as functions of the factorization/renormalization scale in Fig.2(a) and Fig.3(a), respectively. There we set $\mu \equiv \mu_f = \mu_r$ and take the LED parameters as $M_S = 4.8$ TeV and $d = 3$. We can read out from Fig.2(a) and Fig.3(a) that the K -factors range from 2.04 to 1.85 and from 2.40 to 2.06 for the ZZW^+ and ZZW^- productions, respectively, with the increment of μ from $0.25\mu_0$ to $4\mu_0$. We also find that the LO cross section underestimates the scale uncertainty, because the ZZW^+ and ZZW^- productions at the LO are pure electroweak processes, and the LO scale uncertainty is apparently only related to the PDFs. While the NLO scale uncertainty is related to both the factorization scale and the renormalization scale, and is enhanced obviously due to $\alpha_s(\mu_r)$ appearing at the NLO.

For demonstrating the main origin of the scale uncertainty, we plot the NLO QCD corrected total cross sections, Born contributions, real light-quark emission and virtual plus real gluon emission correction components for the ZZW^+ and ZZW^- productions in the LED model at the $\sqrt{s} = 14$ TeV LHC versus the scale μ in Fig.2(b) and Fig.3(b), respectively. From these figures we can see that the NLO scale uncertainties for both the ZZW^+ and the ZZW^- production processes are mainly induced by the real

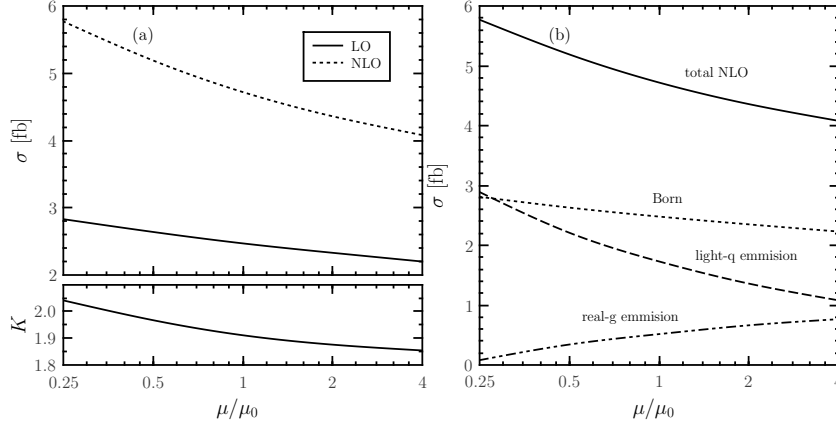


Figure 2: Scale dependence of the LO and NLO QCD corrected cross sections for the $pp \rightarrow ZZW^+ + X$ process at the $\sqrt{s} = 14$ TeV LHC in the LED model. (a) Integrated LO, NLO QCD corrected cross sections and the corresponding K -factors. (b) Different contribution parts to the NLO total cross section.

light-quark emission corrections, which originate from the gluon-initiated subprocesses, and are mainly responsible for the large value of K -factor.

III.4 LED parameter dependence

In Table 5, we list the LO, NLO QCD corrected integrated cross sections and the corresponding K -factors for the ZZW^+ and ZZW^- productions in the LED model at the 14 TeV LHC for some typical values of M_S and d . We can see that the integrated cross section in the LED model decreases with the increment of M_S and approaches to the corresponding SM prediction. On the other hand, for a fixed value of M_S the deviation between the predictions in the LED model and the SM increases when the value of d becomes smaller. It can be ascribed to the fact that the contribution of the interchanging KK-graviton is reduced with the increment of M_S and/or d (see Eq.(2.1)), as shown explicitly in the KK-graviton propagator listed in Table 1.

III.5 LED effects on differential distributions

To describe the LED effect on the differential distribution with respect to a kinematic variable x , we introduce a quantity named LED relative discrepancy defined as $\delta(x) = \left(\frac{d\sigma_{LED}}{dx} - \frac{d\sigma_{SM}}{dx} \right) / \frac{d\sigma_{SM}}{dx}$. Due to the CP -conservation, the difference between the observables for the ZZW^+ production and those for the ZZW^- production at the LHC only comes from the different PDFs of the incoming partons. Therefore, we provide only the kinematic distributions for the $pp \rightarrow ZZW^+ + X$ process as a representative in

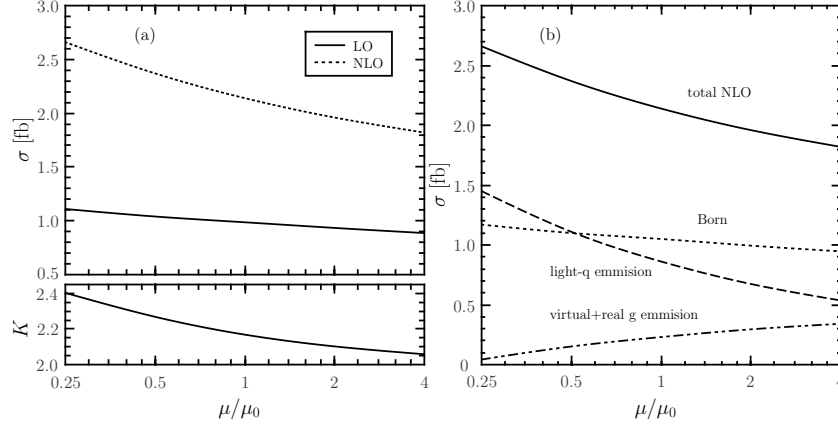


Figure 3: Scale dependence of the LO and NLO QCD corrected cross sections for the $pp \rightarrow ZZW^- + X$ process at the $\sqrt{s} = 14$ TeV LHC in the LED model. (a) Integrated LO, NLO QCD corrected cross sections and the corresponding K -factors. (b) Different contribution parts to the NLO total cross section.

M_S (TeV)	$d = 3$			$d = 4$			$d = 5$		
	σ_{LO} (fb)	σ_{NLO} (fb)	K	σ_{LO} (fb)	σ_{NLO} (fb)	K	σ_{LO} (fb)	σ_{NLO} (fb)	K
5	2.374(2)	4.649(5)	1.959	2.276(1)	4.556(6)	2.002	2.220(1)	4.508(6)	2.030
5.5	2.228(1)	4.527(6)	2.032	2.172(1)	4.468(6)	2.057	2.142(1)	4.439(6)	2.072
6	2.155(1)	4.461(7)	2.070	2.122(1)	4.436(5)	2.091	2.104(1)	4.411(6)	2.097
6.5	2.117(1)	4.435(6)	2.095	2.097(1)	4.418(5)	2.107	2.085(1)	4.404(6)	2.112

M_S (TeV)	$d = 3$			$d = 4$			$d = 5$		
	σ_{LO} (fb)	σ_{NLO} (fb)	K	σ_{LO} (fb)	σ_{NLO} (fb)	K	σ_{LO} (fb)	σ_{NLO} (fb)	K
5	0.961(1)	2.115(3)	2.201	0.934(1)	2.085(3)	2.232	0.919(1)	2.065(3)	2.247
5.5	0.923(1)	2.075(3)	2.247	0.908(1)	2.059(3)	2.269	0.899(1)	2.047(3)	2.276
6	0.904(1)	2.056(3)	2.273	0.895(1)	2.046(3)	2.288	0.889(1)	2.040(3)	2.294
6.5	0.894(1)	2.050(3)	2.293	0.888(1)	2.038(3)	2.295	0.885(1)	2.036(3)	2.301

Table 5: The LO, NLO QCD corrected cross sections and the corresponding K -factors for the $pp \rightarrow ZZW^+ + X$ (upper table) and $pp \rightarrow ZZW^- + X$ (lower table) processes in the LED model with $\mu = \mu_0$ at the $\sqrt{s} = 14$ TeV LHC for some typical values of M_S and d .

further discussion.

Due to the symmetric feature of the rapidity y we study the behaviour of the rapidity distribution only in the positive rapidity region ($y \in [0, 3]$) in following discussions. In Figs.4(a, b), we provide the LO, NLO QCD corrected transverse momentum and rapidity distributions of final W^+ -boson for the ZZW^+ production at the $\sqrt{s} = 14$ TeV LHC in both the SM and the LED model. The corresponding K -factors and the LED relative discrepancies are also plotted in these figures. As shown in Fig.4(a), the LED effect becomes larger with the increment of $p_T^{W^+}$. The LO LED relative discrepancy $\delta_{LO}(p_T^{W^+})$ ranges from 14.3% to 27.5% in the region of $20 \text{ GeV} < p_T^{W^+} < 300 \text{ GeV}$, while $\delta_{NLO}(p_T^{W^+})$, which is heavily suppressed by the NLO QCD corrections, goes up from 7.15% to 8.82% in the same $p_T^{W^+}$ region. From Fig.4(b) we can see that $\delta_{LO}(y^{W^+})$ in the range of $y^{W^+} \in [0, 3]$ is larger than 8% and has its maximum of about 28.2% at $y^{W^+} = 0$, while $\delta_{NLO}(y^{W^+})$, which is remarkably suppressed, ranges from 6.38% to 9.97% in the region of $0 < y^{W^+} < 3$. Both the two figures show that the NLO QCD correction is significant, and the K -factors exceed 1.5 in both the SM and the LED model in the plotted $p_T^{W^+}$ and y^{W^+} regions.

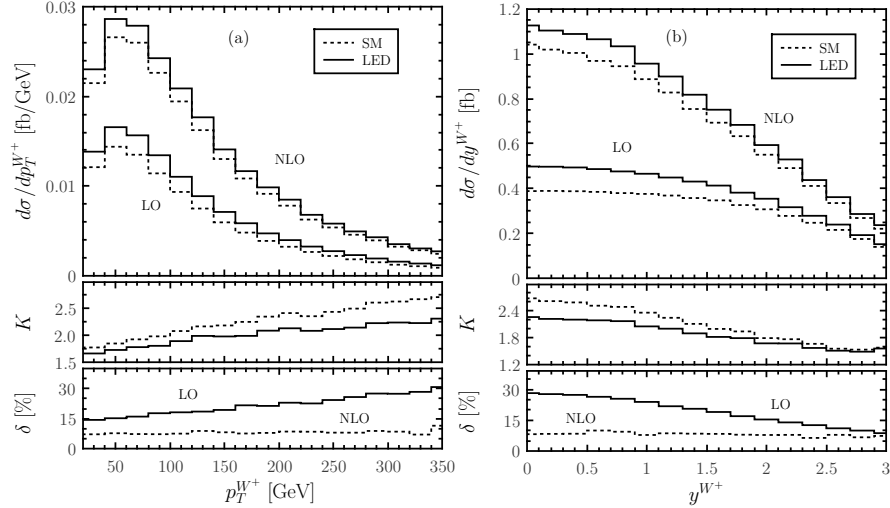


Figure 4: The LO and NLO QCD corrected kinematic distributions of final W^+ -boson for the ZZW^+ production at the $\sqrt{s} = 14$ TeV LHC in both the SM and the LED model, and the corresponding K -factors and the LED relative discrepancies. (a) $p_T^{W^+}$ distributions. (b) y^{W^+} distributions.

The transverse momentum and rapidity distributions of final two Z -bosons for the $pp \rightarrow ZZW^+ + X$ process at the $\sqrt{s} = 14$ TeV LHC, are depicted in Fig.5(a) and Fig.5(b), respectively. In these figures we pick p_T^Z and y^Z of each of the two identical Z -bosons as an entry in the histograms, then the final

differential cross section should be multiplied by $\frac{1}{2}$. The corresponding K -factors and the LED relative discrepancies are depicted in the lower plots of Figs.5(a, b). We can read out from Fig.5(a) that both the LO and the NLO LED relative discrepancies are less than 10% in the region of $p_T^Z \in [100, 400]$ GeV, but they grow up quickly and become to be very large, when p_T^Z goes up beyond 400 GeV. That is because the LED contributions induced by the KK gravitons enhance the differential distributions. As shown in Fig.5(b), the y^Z distributions are similar to the y^{W^+} distributions shown in Fig.4(b), and the significant LED contributions are concentrated in low y^Z region. The LO and NLO QCD corrected LED relative discrepancies reach their maxima of about 35.77% and 13.05% at $y^Z = 0$, respectively.

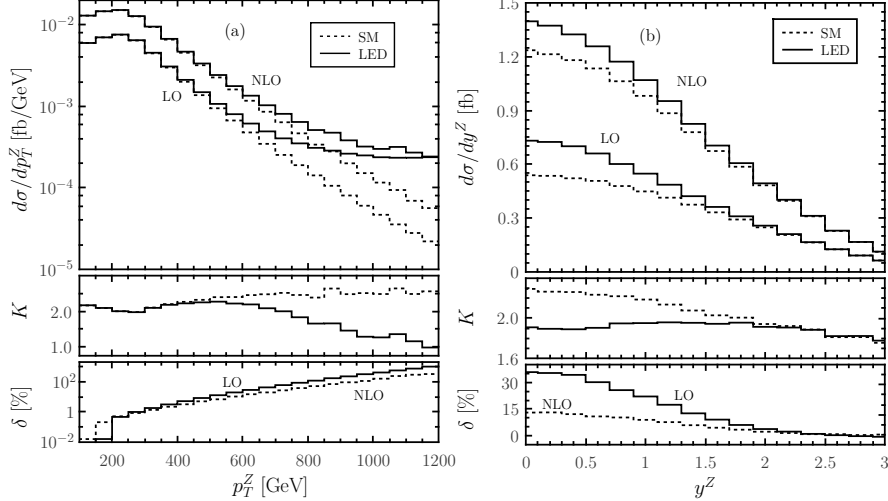


Figure 5: The LO and NLO QCD corrected kinematic distributions of final Z -bosons for the ZZW^+ production at the $\sqrt{s} = 14$ TeV LHC in both the SM and the LED model, and the corresponding K -factors and the LED relative discrepancies. (a) p_T^Z distributions. (b) y^Z distributions.

In Fig.6 we present the LO and NLO QCD corrected distributions of the Z -boson pair invariant mass M_{ZZ} for the $pp \rightarrow ZZW^+ + X$ process at the $\sqrt{s} = 14$ TeV LHC in both the SM and the LED model, and the corresponding K -factors and the LED relative discrepancies are shown in the lower plots. It shows that the LED effect increases rapidly as the increment of M_{ZZ} , while is very small in relatively low M_{ZZ} region. This behavior of the M_{ZZ} distribution can be interpreted as that the contribution of the KK-graviton propagator increases distinctly with the increment of M_{ZZ} since the KK graviton interacts directly with the final Z -boson pair (see Eq.(2.1) and Fig.1). When M_{ZZ} goes beyond 2.5 TeV, K -factors approach to 1 in both SM and the LED model.

All the above kinematic distributions show that the LED effect could be significant for ZZW pro-

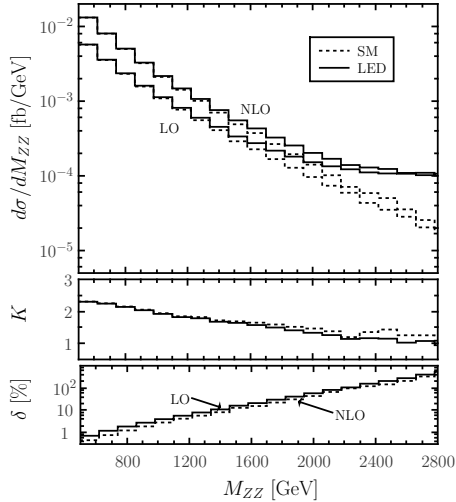


Figure 6: The LO and NLO QCD corrected distributions of the Z -boson pair invariant mass for the ZZW^+ production at the $\sqrt{s} = 14$ TeV LHC in both the SM and the LED model, and the corresponding K -factors and the LED relative discrepancies.

duction at the 14 TeV LHC by adopting proper event selection criteria, particularly in the high p_T , central rapidity y and large M_{ZZ} regions, the LED effect becomes to be evidently large. We see that after including the NLO QCD corrections, the LED effect is reduced remarkably. We conclude that the LO result for the ZZW production at the 14 TeV LHC overestimates the LED effect.

IV. Summary

We investigate the LED effect induced by the KK gravitons on the ZZW production at the $\sqrt{s} = 14$ TeV LHC up to the QCD NLO. We also study the factorization/renormalization scale dependence of the total cross section and show that the LO prediction underestimates the scale uncertainty. Some kinematic distributions are provided in both the SM and the LED model. Our numerical results demonstrate that the NLO QCD corrections are sizeable and reduce the LED effect remarkably, and the NLO QCD correction and the LED effect are strongly related to phase space. We conclude that the LO result overestimates the LED effect and is insufficient to provide a believable theoretical prediction in the LED model, and the NLO LED relative discrepancy of the total cross section could become sizable for the ZZW production by adopting proper event selection scheme.

Acknowledgments: Thanks for the help and support of Supercomputing center of USTC in our numerical calculations. This work was supported in part by the National Natural Science Foundation of

China (Grants. No.11275190, No.11375008, No.11375171).

References

- [1] N. Arkani-Hamed, S. Dimopoulos, G. Dvali, Phys. Lett. **B429** (1998) 263.
- [2] N. Arkani-Hamed, S. Dimopoulos, G. Dvali, Phys. Rev. **D59** (1999) 086004.
- [3] I. Antoniadis, N. Arkani-Hamed, S. Dimopoulos, G. Dvali, Phys.Lett. **B436** (1998) 257.
- [4] T. Han, J. D. Lykken, R. -J. Zhang, Phys. Rev. **D59** (1999) 105006.
- [5] S. Godfrey, arXiv:hep-ph/9505252.
- [6] O. J. P. Eboli, M. C. Gonzalez-Garcia, S. M. Lietti, Phys. Rev. **D69** (2004) 095005.
- [7] O. J. P. Éboli, M. C. Gonzalez-Garcia, S. M. Lietti, S. F. Novaes, Phys. Rev. **D63** (2001) 075008.
- [8] D. Green, arXiv:hep-ex/0310004.
- [9] M. C. Kumar, P. Mathews, V. Ravindran, S. Seth, Phys. Rev. **D85** (2012) 094507.
- [10] X. -Z. Li, P. -F. Duan, W. -G. Ma, R. -Y. Zhang, L. Guo, Phys. Rev. **D86** (2012) 095008.
- [11] R. Franceschini, Mod. Phys. Lett. **A28** (2013) 1330008.
- [12] G. F. Giudice, R. Rattazzi, J. D. Wells, Nucl. Phys. **B544** (1999) 3.
- [13] Y. -M. Bai, L. Guo, X. -Z. Li, W. -G. Ma, R.-Y. Zhang, Phys. Rev. **D85** (2012) 016008.
- [14] T. Hahn, Comput. Phys. Commun. **140** (2001) 418.
- [15] T. Hahn, M. Perez-Victoria, Comput. Phys. Commun. **118** (1999) 153.
- [16] F. Campanario, V. Hankele, C. Oleari, S. Prestel, D. Zeppenfeld, Phys. Rev. **D78** (2008) 094012.
- [17] T. Binoth, G. Ossola, C. G. Papadopoulos, R. Pittau, JHEP **06** (2008) 082.
- [18] G. Passarino, M. J. G. Veltman, Nucl. Phys. **B160** (1979) 151.
- [19] A. Denner, S. Dittmaier, Nucl. Phys. **B658** (2003) 175.

- [20] Fawzi Boudjema, Le Duc Ninh, Sun Hao, Marcus M. Weber, Phys. Rev. **D81** (2010) 073007.
- [21] Fawzi Boudjema, Le Duc Ninh, Sun Hao, Marcus M. Weber, proceedings of the 3rd CPP Workshop, September 23-25, 2010, KEK Tsukuba Japan, arXiv:1101.0359.
- [22] S. Catani, M. H. Seymour, Nucl. Phys. **B485** (1997) 291; Erratum-ibid. **B510** (1998) 503.
- [23] Z. Nagy, Phys. Rev. **D68** (2003) 094002.
- [24] J. Beringer *et al.* [Particle Data Group], Phys. Rev. **D86** (2012) 010001.
- [25] G. Aad *et al.* [ATLAS Collaboration], Phys. Lett. **B716** (2012) 1.
- [26] S. Chatrchyan *et al.* [CMS Collaboration], Phys. Lett. **B716** (2012) 30.
- [27] J. Pumplin, D. R. Stump, J. Huston, H. L. Lai, P. Nadolsky, W. K. Tung, JHEP **07** (2002) 012.
- [28] G. Aad *et al.* [ATLAS Collaboration], New J. Phys. **15** (2013) 043007.
- [29] G. Aad *et al.* [ATLAS Collaboration], Phys. Rev. **D87** (2013) 015010.
- [30] S. Chatrchyan *et al.* [CMS Collaboration], CMS Physics Analysis Summary, CMS PAS EXO-12-031.